Article

ASTER-Based Remote Sensing Image Analysis for Prospection Criteria of Podiform Chromite at the Khoy Ophiolite (NW Iran)

Behnam Mehdikhani and Ali Imamalipour *

Department of Mining Engineering, Urmia University, Urmia 57561-51818, Iran; b.mehdikhani@urmia.ac.ir
* Correspondence: A.imamalipour@urmia.ac.ir

Abstract: A single chromite deposit occurrence is found in the serpentinized harzburgite unit of the Khoy ophiolite complex in northwest Iran, which is surrounded by dunite envelopes. This area has mountainous features and extremely rugged topography with difficult access, so prospecting for chromite deposits by conventional geological mapping is challenging. Therefore, using remote sensing techniques is very useful and effective, in terms of saving costs and time, to determine the chromite-bearing zones. This study evaluated the discrimination of chromite-bearing mineralized zones within the Khoy ophiolite complex by analyzing the capabilities of ASTER satellite data. Spectral transformation methods such as optimum index factor (OIF), band ratio (BR), spectral angle mapper (SAM), and principal component analysis (PCA) were applied on the ASTER bands for lithological mapping. Many chromitite lenses are scattered in this ophiolite, but only a few have been explored. ASTER bands contain improved spectral characteristics and higher spatial resolution for detecting serpentinized dunite in ophiolitic complexes. In this study, after the correction of ASTER data, many conventional techniques were used. A specialized optimum index factor RGB (8, 6, 3) was developed using ASTER bands to differentiate lithological units. The color composition of band ratios such as RGB $((4+2)/3, (7+5)/6, (9+7)/8)$, $(4/1, 4/7, 4/5)$, and $(4/3 \times 2/3, 3/4, 4/7)$ produced the best results. The integration of information extracted from the image processing algorithms used in this study mapped most of the lithological units of the Khoy ophiolitic complex and new prospecting targets for chromite exploration were determined. Furthermore, the results were verified by comprehensive fieldwork and previous studies in the study area. The results of this study indicate that the integration of information extracted from the image processing algorithms could be a broadly applicable tool for chromite prospecting and lithological mapping in mountainous and inaccessible regions such as Iranian ophiolitic zones.

Keywords: ASTER; chromite; Khoy ophiolite; spectral angle mapper (SAM); band ratio; principal component analysis (PCA)

1. Introduction

The mapping of ophiolite sequences has become a research interest of scientists and exploration geologists in the world because they host economic minerals such as chromium, copper, manganese, gold, nickel, barium, lead, and zinc [1–3]. Ophiolitic ultramafic rocks are the hosts of podiform chromite deposits. Podiform chromite deposits are small magmatic chromite bodies formed in the lower level of an ophiolite complex. Podiform chromite mines have produced 57.4% of the world's total chromite production [4]. Ophiolite zones in Iran are widespread and are often found in different locations with varying geologic and tectonic settings. The Khoy ophiolite complex is a part of the Tethyan ophiolite belt, and it is one of the largest Iranian ophiolite complexes, covering a widespread area in northwest Iran along the Iran–Turkey border and continuing toward western Turkey [5,6]. Ultramafic rocks, which are often serpentinized, are widespread in 250 km^2 of the Khoy ophiolite [5,6]. The Khoy ophiolite is one of the most promising areas for prospecting chromite deposits because of extensive outcrops of ultramafic rocks. So far, more than

20 chromite deposits have been identified in this area. These chromite occurrences have lenticular, tubular, and vein-like shapes hosted by serpentinized harzburgite. The chromite deposits in the Khoy ophiolite can be clearly classified into two groups: high-Al chromites (Cr# = 0.38–0.44) from the eastern ophiolite, and high-Cr chromites (#Cr = 0.54–0.72) from the western ophiolite [5,6]. Most Iranian ophiolitic zones are located in mountainous and inaccessible regions. Thus, prospecting for chromite deposits with geological mapping is challenging and time-consuming.

Remote sensing analysis plays an important role in the exploration of mineral deposits, as well as in lithological mapping and detection of associated hydrothermal mineralization, in Iran. The Advanced Spaceborne Thermal Emission and Reflection Radiometer (ASTER) is an advanced multispectral satellite imaging system that has created new tools for the mapping of geological structures and detecting certain alteration minerals or assemblages [2,3,7].

The ASTER sensor launched the TERRA platform in December 1999. The ASTER platform travels in a near-circular, sun-synchronous orbit with an inclination of approximately 98.2°, an altitude of 705 km, and a repeat cycle of 16 days, offering relatively improved spatial, spectral, and temporal resolutions. It is made from three visible and near-infrared spectral bands (VNIR, between 0.52 and 0.86 μm, with 15-m spatial resolution) and infrared, reflecting radiation in six short-wavelength infrared spectral bands (SWIR, between 1.6 and 2.43 μm, with 30 m spatial resolution). Sensor characteristics of the ASTER instruments are shown in Table 1 [8,9].

Table 1. Sensor characteristics of ASTER instruments [8].

Sensor Characteristics	ASTER					
	VNIR		SWIR		TIR	
	Band01	0.52–0.60	Band04	1.6–1.7	Band10	8.125–8.475
	Band02	0.63–0.69	Band05	2.45–2.185	Band11	8.475–8.825
Spectral bandswith range (μm)	Band03N	0.76–0.86	Band06	2.185–2.225	Band12	8.925–9.275
	Band03B	0.76–0.86	Band07	2.235–2.285	Band13	10.95–10.95
	Backward-looking		Band08	2.2295–2.365	Band14	10.95–11.65
			Band09	2.36–2.43		
Spatial resolution (m)	15		30		90	
Swathwidth (km)	60		60		60	

Due to the great extent of ultramafic rocks, which are the host of chromite deposits in the Khoy ophiolite, the possibility of discovering new chromite deposits is high and more exploration and investigation is needed. Given the extremely rugged topography with difficult access, new exploration methods such as the remote sensing method can be useful for this purpose. The present study evaluates the discrimination of chromite-bearing mineralized zones within the Khoy ophiolite complex by analyzing the capabilities of ASTER satellite data. Advanced Spaceborne Thermal Emission and Reflection Radiometer (ASTER) data can easily separate various rock units, the extent of the ultramafic rocks, and it can provide detailed geological maps of the area [8,9].

The extraction of spectral information related to ophiolite mapping can be achieved through image processing techniques such as band ratio (BR) and principal component analysis (PCA) on ASTER bands [8,10]. The color composition of the band ratio (4/1, 4/5, 4/7) is an effective means of determining the lithological ophiolite complexes [11].

Principle component analysis and band ratio methods are very useful for determining the serpentinized dunite that is the host of the chromite veins [7,11–14]. Abdeen used ASTER spectral band ratios RGB color composite of 4/7, 4/1, 2/3, 4/3, and RGB (4/7, 3/4, 2/1) for mapping ophiolitic units, metasediments, volcanoclastic, and granitoids in the southeastern desert of Egypt [15]. Amer used principal component analysis of ASTER data to determine the lithologic units of the ophiolite complexes in Pakistan. In the eastern ophiolites of Egypt, Amer used band ratios of (7 + 9)/8, (5 + 7)/6, (2 + 4)/3,

and PCA (4,5,2) for the lithological mapping of several units [7]. Hashem and Pournamdari conducted research using ASTER data on the Abdasht ophiolites in northeastern Iran [12]. Thermal infrared (TIR) bands in the thermal range of spectral absorption can be used for the detection of silicate formations [16].

2. Description of the Study Area

The Khoy ophiolite covers an area of about 3900 km^2 in northwest Iran along the Iran–Turkey boundary. This ophiolitic complex is limited on the west and north by the Iran–Turkey border and on the east and south by a southeastern-northeastern fault (Figure 1). This zone reaches the Urmia Lake platform on the south. Precambrian metamorphic rocks including meta-volcanic, amphibolite, gneiss, and the Precambrian Kahar formation with the Rb-Sr age of 663 Ma [17] are the oldest rocks in this area and are located in the eastern portion of the ophiolite zone. It seems that this ophiolite is the remnant of a branch of the Neotethyan oceanic basin. It is joined to the northeast ophiolite of Turkey in the Western Pontides. The only reported age for this ophiolite is 81.2 ± 2.1 to 69.4 ± 1.6 Ma [18].
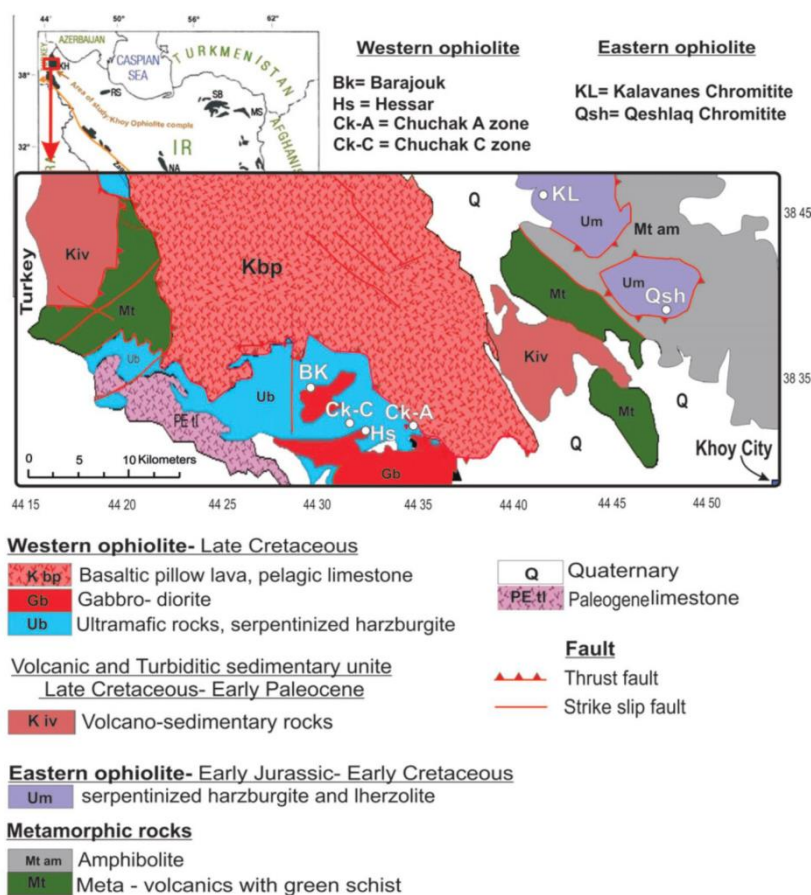

Figure 1. Geological map of the study area (modified after Khoy 1:250,000 geological map) and sample locations associated with a sketched map of Iran showing locations of some of the most important ophiolites in Iran [6,19]. KH, Khoy; MS, Mashhad; RS, Rasht; SB, Sabzevar.

New geochemical and field studies on the ophiolite of Khoy indicate that there are two ophiolite complexes in this area with different geological ages: (i) the early Jurassic to early Cretaceous eastern Khoy ophiolite and (ii) the late Cretaceous western Khoy ophiolite. The second one is a remnant of the Neotethyan oceanic crust [18,19]. The Khoy ophiolite has all the parts of an ophiolite sequence. It is composed of serpentinized peridotite, layered and isotropic gabbro, isolated diabasic dike, pillow basalt, massive sheet flow, and interbedded hyaloclastic breccia and tuffs. Ultramafic rocks have been

cut by rodengitic dikes. The Khoy ophiolite was unconformably covered by Eocene rocks, including limestone, marl, and conglomerate. Associated with ophiolitic rocks are found flysch-type sediments with Paleocene-lower Eocene age that have syn-orogenic characteristics. After emplacement of the ophiolitic complex at the end of post-lower Eocene age, acidic to intermediate magmatic activity, as small granitoid intrusive rocks and andesitic-dacitic volcanic and their sub-volcanic equivalents, occurred [5,6].

The serpentinized harzburgites and related rocks in the western Khoy ophiolite are intruded on by gabbro–diorite intrusions, which appear as a spot inside and/or around serpentinized harzburgites and cannot be a member of the ophiolite sequence [6]. Ultramafic rocks of the western Khoy ophiolite host several podiform chromitite bodies. The chromite deposits have lenticular, tabular, and irregular vein shapes and are emplaced in depleted mantle harzburgite [5,6]. The recognized outcrops altogether are discordant with their harzburgite host rocks. Chromite bodies are surrounded by dunitic envelopes with variable thicknesses. The existence of a dunitic envelope with various thicknesses is a common characteristic of all chromite ore bodies in this area. Most of them are small and contain little reserves, and only the Aland, Qeshlag, and Kochek deposits, with several tens of thousands of reserves, are minable [5,6].

3. ASTER Satellite Data

This paper aims to evaluate the accuracy of ASTER images for targeting the discrimination of chromite-bearing mineralized zones within the serpentinized harzburgite rocks in an extensive area of the Khoy ophiolite complex.

The ASTER data in this study were obtained from the Earth and Remote Sensing Data Analysis Center (ERSDAC) in Japan and consist of a level 1B scene acquired in 2002. The images have been georeferenced to UTM zone 38 North projections with the WGS-84 datum. Atmospheric correction on the VNIR and SWIR bands was applied by the log residual method. Finally, correlation coefficient, optimum index factor, principal component analysis, and band ratio were evaluated for lithological mapping in this study. Figure 2 shows the serpentinite, chromite, and pillow lava in the study area.
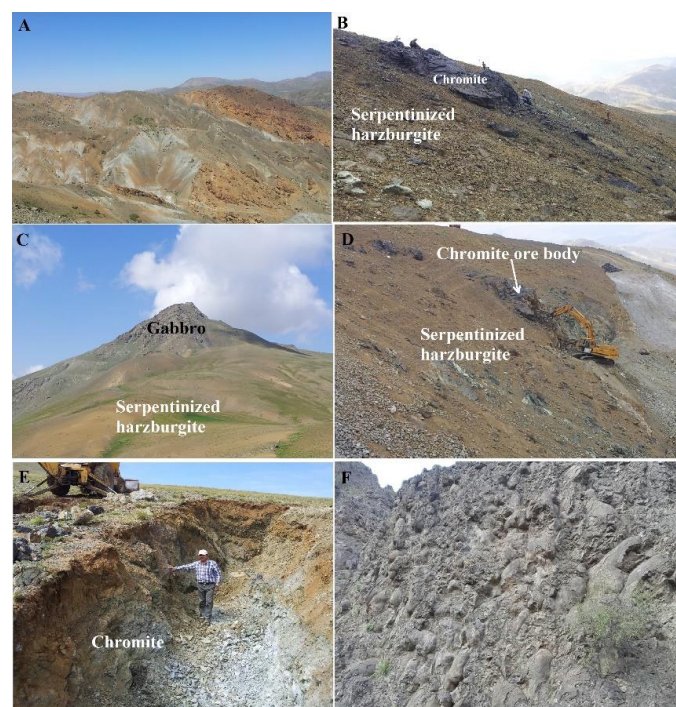

Figure 2. Field photographs show: (**A**) serpentinized harzburgite; (**B**) lens-shaped chromite within serpentinized harzburgite; (**C**) gabbroic intrusion within the ultramafic rocks; (**D**) chromite ore body; (**E**) chromite ore body within serpentinized harzburgite covered by overburden; (**F**) basaltic pillow lava.

4. Ophiolite Spectral Properties

The spectral reflectance of a rock depends on the type of mineralogical composition of the whole rock. The absorption of minerals also depends on the number of electronic processes occurring in these rocks [20]. Recent studies on the number of reflections from the surface of rocks have provided very important aspects of the study of remote sensing data. Many researchers utilized remote sensing and GIS techniques for lithological mapping as well as identifying mineral deposits [9,10,21–24].

Sabins concluded that remote sensing techniques can be used for mineral explorations in four ways: (1) Mapping of faults and structures that deposits can form in that trend; (2) mapping local fractures that may control ore deposits individually; (3) alteration of mapping in altered rocks associated with mineralization; and (4) providing geological base maps to start explorations [10]. In laboratory studies, the reflection spectrum of some of the rocks of various ophiolite units was studied by Abrams [21]. Figure 3 shows the spectral measurements of minerals found in harzburgites and gabbros [25].
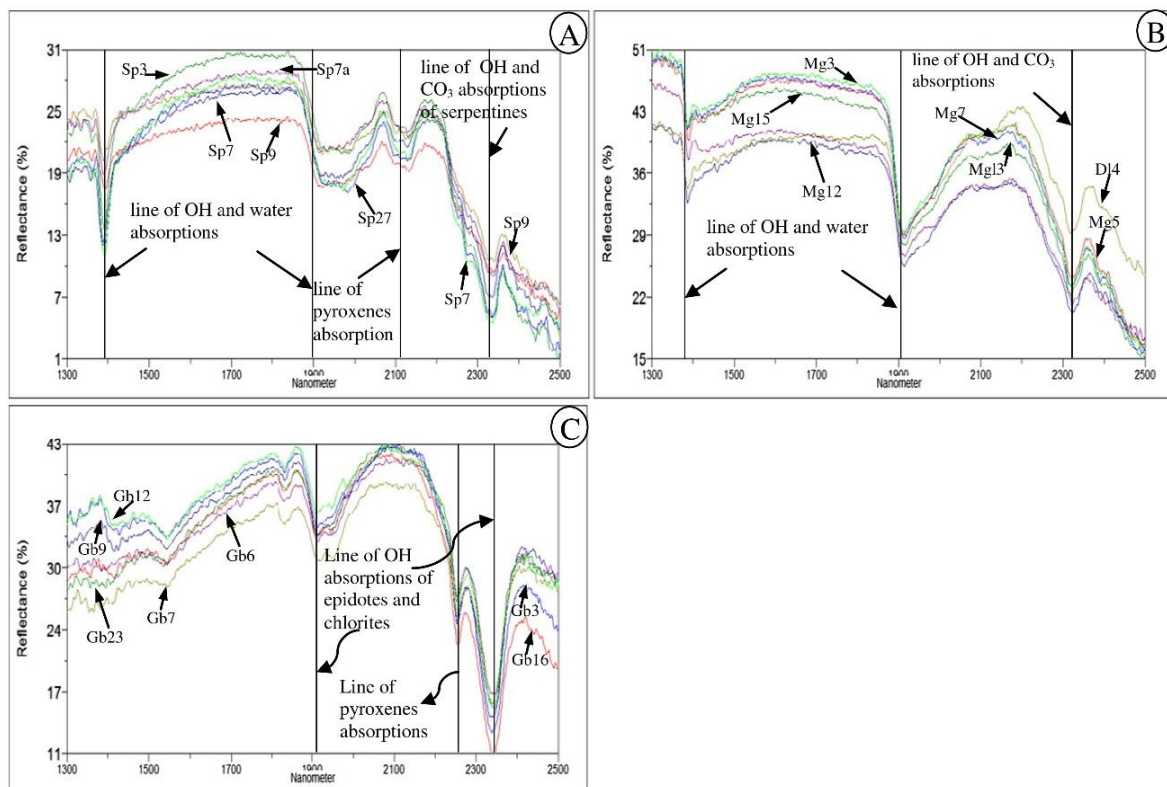

Figure 3. Spectral plots of (**A**) the harzburgites; (**B**) the harzburgites with carbonates; (**C**) the gabbros [25].

5. Methodology

To delineate the area of chromite mineralized zones within the serpentinized harzburgite, a host of chromitite in the Khoy ophiolite area, the ASTER satellite's images were processed. The first stage in the exploration program was finding the harzburgite and dunite lithologies. Methods such as the different band rationing method and principal component analysis techniques, which were tested in scientific publications on the mapping of ophiolites, were used. In this study, a regional geology map was used to support the remote sensing studies. Before any processing on ASTER data, some preprocessing—including topography, atmospheric, radiometric, and geometric corrections—had to be carried out on their bands.

The ASTER, with two data series of VNIR and SWIR for the separation of the lithology units, yielded very good results [15,24]. The selection of different band ratios was based on the spectral reflectance of rocks and their minerals, and such band ratio images, designed to display the spectral contrast of specific absorption features, can be used extensively in geological remote sensing. The band ratio method is frequently used in lithological mapping and mineral exploration using remote sensing data [7,23,26–31]. Additionally, the ASTER band ratio is suitable for the exploration and detection of serpentinite dunite and harzburgite of ophiolite [9,12,13,15]. Iron oxides, clay minerals, sulfates, and carbonates are some rocks and minerals that can be identified and separated by ASTER data [13]. Abdeen used ASTER band ratios of 4/7, 4/1, 2/3 × 4/3 and 4/7, 3/4, 2/1 in RGB for mapping ophiolites, metasediments, volcanoclastic, and granitoids, which are lithologic units of the Neoproterozoic-Allaqi suture in the southeastern desert of Egypt [15].

Amer used band ratios of (2 + 4)/3, (5 + 7)/6, and (7 + 9)/8 to distinguish between ophiolite and granite rocks, and was able to map ophiolite rocks, metabasalt, and metagabbro units [7]. They concluded that these new ratios are much better to separate the lithological units of the ophiolites, so in the present study, these new band ratios were used. PCA is a well-known method for lithological and alteration mapping in metallogenic provinces [7,12–14,24,31]. In this technique, the relationship between the spectral responses of target minerals or rocks and numeric values extracted from the eigenvector matrix was used to calculate the principal component images. Using this relationship, one can determine which PCs contain spectral information due to minerals and whether the digital numbers (DNs) of the pixels containing the target minerals had high (bright) or low (dark) values. Crosta and Amer noted that combining the analysis of the principal components that contain the most information and the principal components that contain the least information can provide much more useful data on the separation of lithology and mineralized zones [7,13].

5.1. Optimum Index Factor (OIF)

The total VNIR and SWIR bands of the ASTER data included 63 different band combinations, with bands 3, 6, and 8 having the highest OIF. Using the combination of different bands caused an increase in the spectral accuracy of the low-correlation bands, especially the thermal bands. Calculations of OIF are required to obtain the best false-color composites (higher OIF color combinations contain more information):

$$OIF = \left(\sum_{i=1}^{3} S_i \right) / \left(\sum_{i=1}^{3} r_i \right) \tag{1}$$

where S_i is the standard deviation in each band, and r_i is a correlation of bands of two to two. Often, the false-color combinations containing the most important information are determined from the variety of colors.

5.2. Spectral Angular Mapper Algorithm

The spectral angle mapping algorithm assumes that a pixel of remote sensing images represents certain ground cover material, which can be uniquely assigned to only one ground cover class. The SAM algorithm is measured based on the degree of similarity between the two spectra. A spectral similarity can include any number of measured spectra (Figure 4). The spectral similarity between two spectra is measured by calculating the angle between the two spectra, treating them as vectors in a space with dimensionality equal to the number of bands [32].
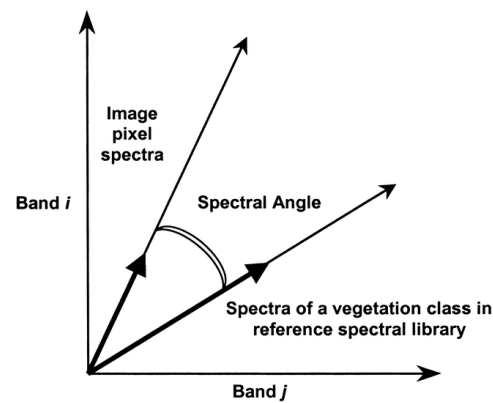
Figure 4. Representation of reference angle [33].

6. Remote Sensing in the Study Area

Optimum index factor (OIF), principal component analysis (PCA), and band ratio (BR) techniques are the spectral angle mapper techniques that were evaluated for lithological mapping in this study [34,35]. The color composition of RGB (8, 6, 3) showed that the spectral accuracy of all bands increased due to the 15 m spectral accuracy of the VNIR band. Figure 5 shows the color composite that distinguishes the serpentine dunites (light green), colored mélange (pink), vegetation (red), and carbonate rocks (yellow).
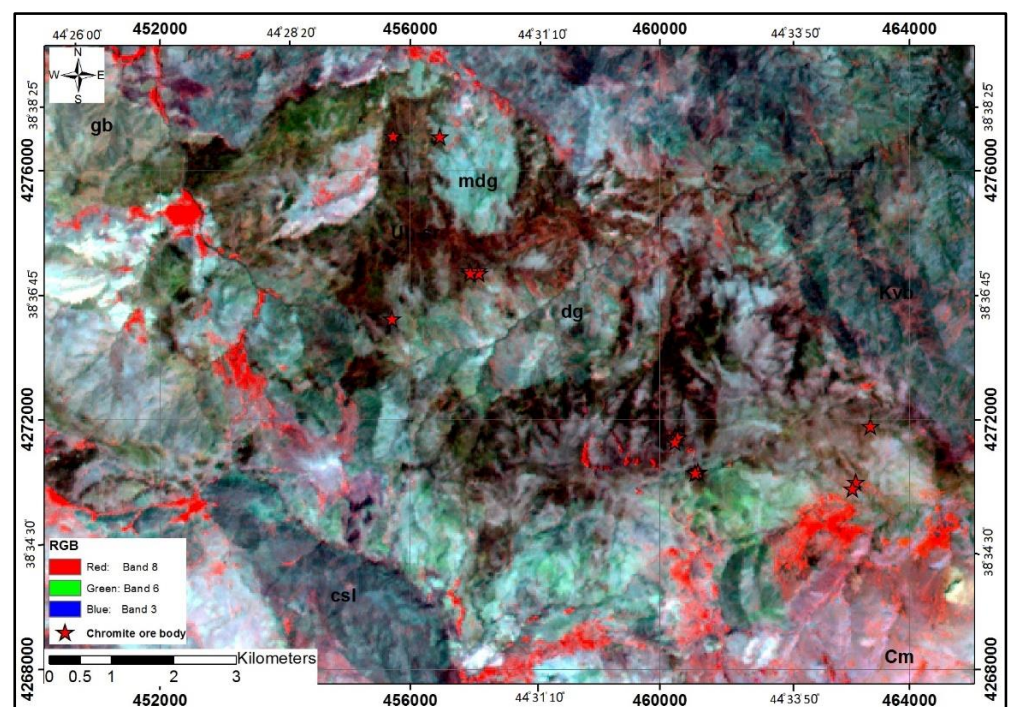
Figure 5. The color composition of RGB (8, 6, 3) from ASTER data after necessary corrections.

The satellite images were projected in the UTM Zone N38 and WGS 1984 ellipsoid (oblate spheroid) datum. For mapping the geology units, we can classify similar pixels using the optimum index factor (OIF), band ratio (BR), etc., and obtain the initial map of the lithology units. By using all available data in the study area, a map of lithological units was obtained (Figure 6).
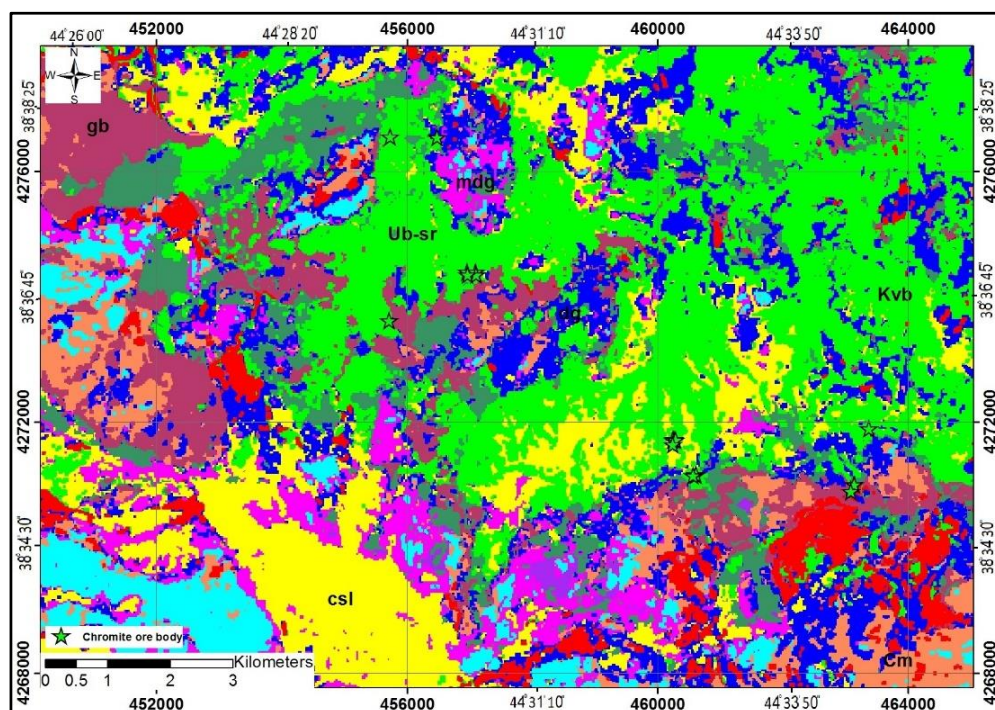
Figure 6. Classified map by using unsupervised classification method from pure pixels.

6.1. Band Ratio

The band ratio method is a suitable technique for lithological mapping, especially to discriminate rock units in ophiolite complexes [7,12,28,30]. For the discrimination of harzburgite rocks (contains more serpentine) and chromite bearing mineralized zones in the study area, all band ratios and their color composites were used, as in Sultan et al. (1986) (5/7, 5/1, 5/4 × 4/3), Sabins (1999) (3/5, 3/1, 5/7), and Gad and Kusky (2007) ((5/3, 5/1, 7/5) and (7/5, 5/4, 3/1)) [10,22,27]. This technique has been used successfully in lithological mappings for other ophiolite areas [7,9,23,26,27,29,30,36]. In the study area, based on the spectral information obtained from the ASTER bands, the color composition of the band ratios (4 + 2)/3, (7 + 5)/6, (7 + 9)/8 in Figure 7 provides the best results in the separation of ophiolite complex lithology units. In this color combination, ultrabasic rocks are pink, and the more serpentinized rocks are reddish. In Khoy ophiolites, there is no specific band ratio for the separation of all units, and several band ratios should be used to distinguish between different lithological units.

An interesting point shown in this figure is the separation of ultrabasic rocks based on the severity of serpentinization. Near the serpentine sections, the serpentinization rate increased sharply and is more reddish. The blue sections are ultrabasic with low serpentinization that is seen far from chromite lenses. The difference between the two types of serpentine spectra is shown in Figure 8. Thus, the severity of serpentinization of ultrabasic rocks can also be considered for the exploration of chromite lenses.
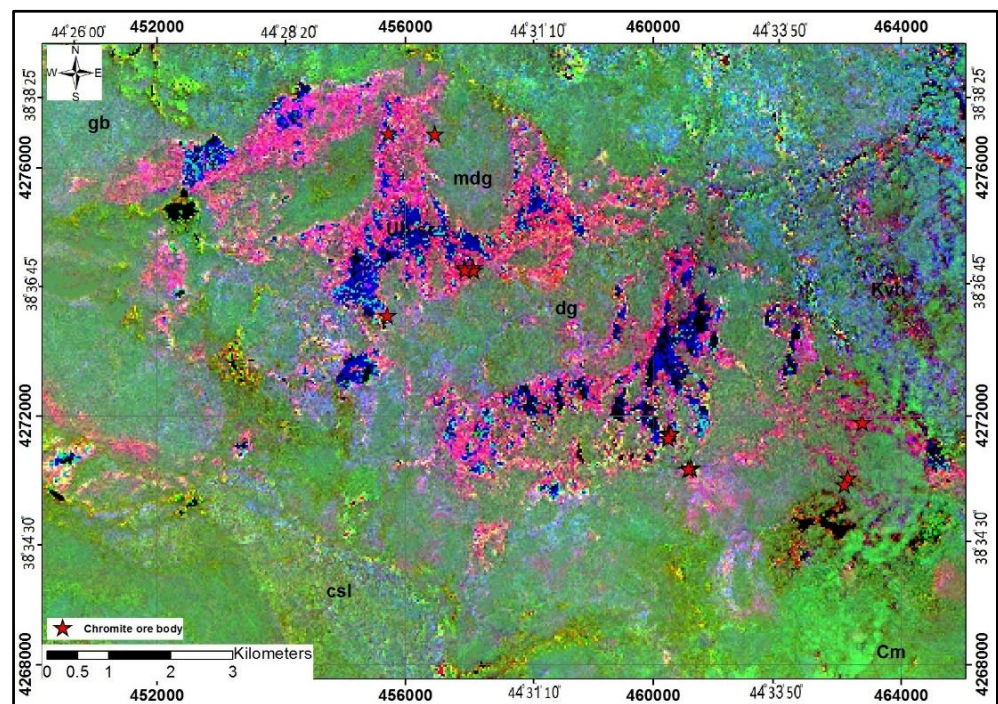
Figure 7. Harzburgite (with slight serpentinization) and highly serpentinized harzburgites (serpentinite) separation.
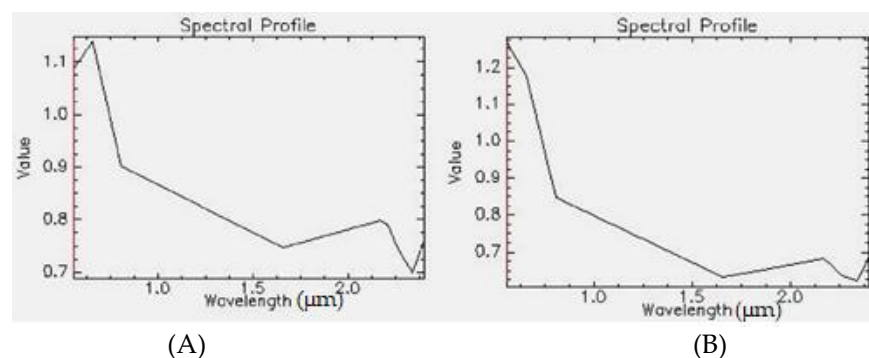

(A)　　　　　　　　　　　　　　　　　　　　　　(B)

Figure 8. Spectral plots of two types of serpentinization intensity: (**A**) high serpentinization; (**B**) low serpentinization.

Therefore, the spectral reflectance in bands two and one is different. As a result, a band ratio of 2/1 can be used to differentiate ultrabasics with different serpentinization intensities. The other band ratio that was considered in this study and can be used to distinguish potential chromite areas is RGB (4/5, 4/7, 4/1), an ultrabasic area characterized by an olive color. Dioritic gabbro is mostly indigo blue, which in the vicinity of ultrabasics is yellowish. Pixels seen at the intersection of these two colors are the best place for points of chromite lenses. All the chromite outcrops in the study area comply with this rule and can be optimized by creating information layers in the GIS software and prioritizing these areas. In this ratio, the conglomerate is mainly purple and is exposed in the southwestern part of the region. In the northwest part of the study area, a gabbro unit is yellow, which is distinguished according to the spectrum obtained from micro gabbro diorite and gabbro-diorite units (Figure 9).
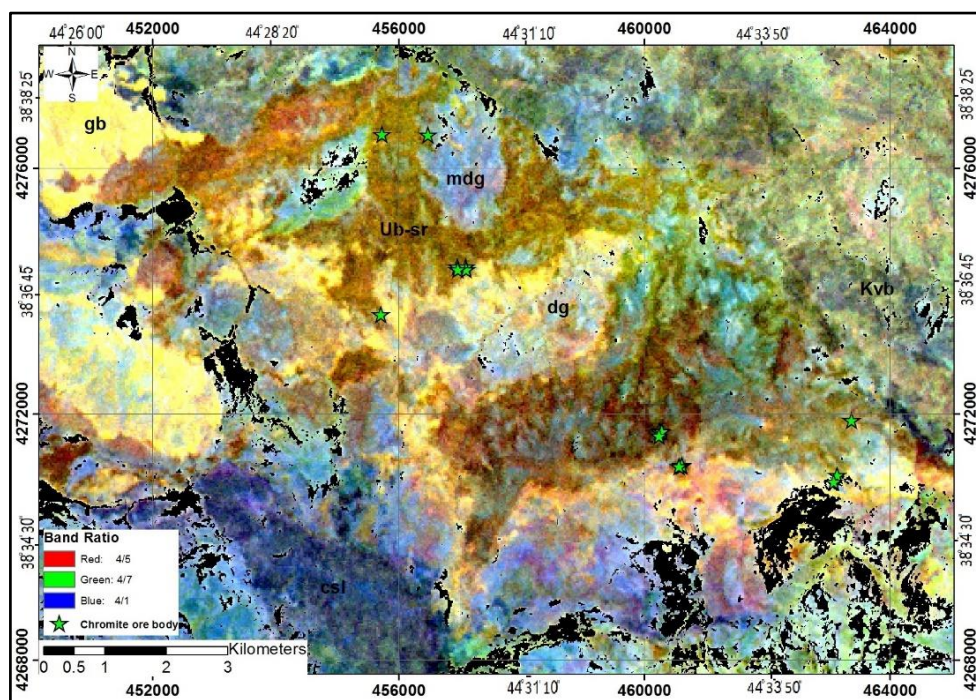
Figure 9. ASTER RGB images of band ratios (4/5, 4/7/4/1) show gabbro-diorite in yellow, serpentinized ultrabasic in purple.

6.2. PCA Analysis

Principal component analysis (PCA) was used to summarize the information in a data set described by multiple variables. Using this technique makes it possible to separate pixels that have good spectral information [13]. In this method, components that have less than 1% of information are deleted due to the high noise in the data. In this study, PCA analysis was applied to all nine bands, and the PCs (1, 2, 3) which included the most information were selected for separation. After PCA calculation, it was found that PC1, PC2, and PC3 had the greatest variances in the data. The eigenvalues for the main components of all ASTER bands are provided in Figure 10.
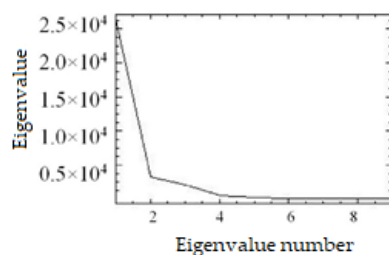
Figure 10. The PCA eigenvalue plot for the VNIR+ SWIR bands of ASTER data.

As a result, the PCA analysis of the VNIR and SWIR bands was used to determine the lithology units of the Khoy ophiolite complexes due to more spectral information. The results showed that PC1 had the highest positive variance. Thus, the PC1 component can provide more information about the lithology and mineralogy of rock units. The PC2 component had the most information from bands three and one, and its bright pixels indicated quartzites. Principal component analysis was also performed on SWIR bands that had information that was not VNIR + SWIR. In the PC4 component, iron and magnesium silicates were distinguished as light pixels. Iron and magnesium silicates such as olivine, iron, and magnesium hydrated phyllosilicates, such as serpentine, have low reflectivity in the visible region and high reflectivity in the NIR [30]. The electron processes cause high

absorption in the VNIR, since cations such as Fe^{2+} and Fe^{3+}, which are often replaced by Mn, Cr, and Ni, are more frequent in the crystalline structure of minerals [20]. PC5 is also very suitable for vegetation mapping because vegetation has a low reflection in band two and a high reflection in band three. In addition, the results showed that PC6 to PC9 was very noisy and lacked proper information. Finally, the color composites of the analysis of PC1, PC2, and PC3 yielded excellent results for the separation of rock units (Figures 11–15).
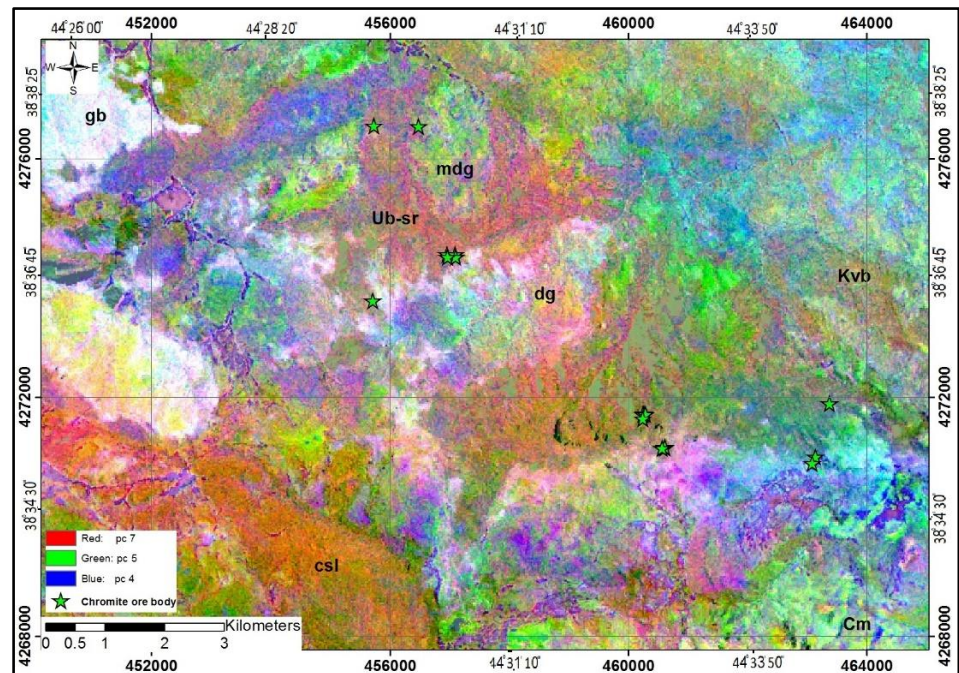
Figure 11. The RGB image of PC7, PC5, and PC4 of PCA bands in the study area.
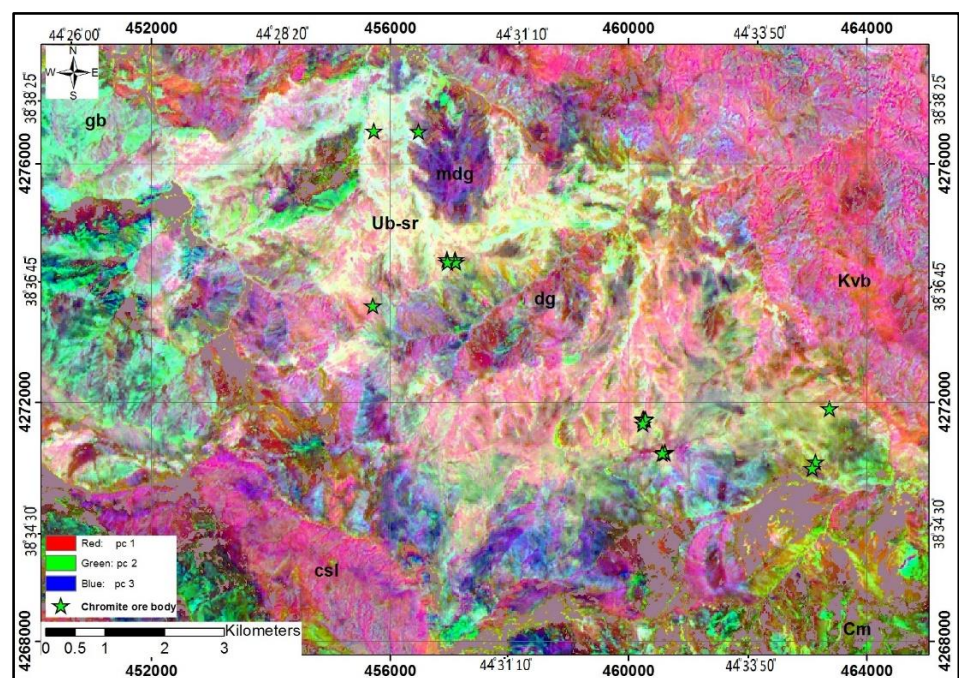
Figure 12. The RGB image of PC1, PC2, and PC3 of PCA bands in the study area: Ub-sr—serpentinized ultrabasic; mdg—microdiorite gabbro; dg—diorite gabbro; Cm—conglomerate; Kvb—basalt pillow lava; csl—shale and conglomerate.
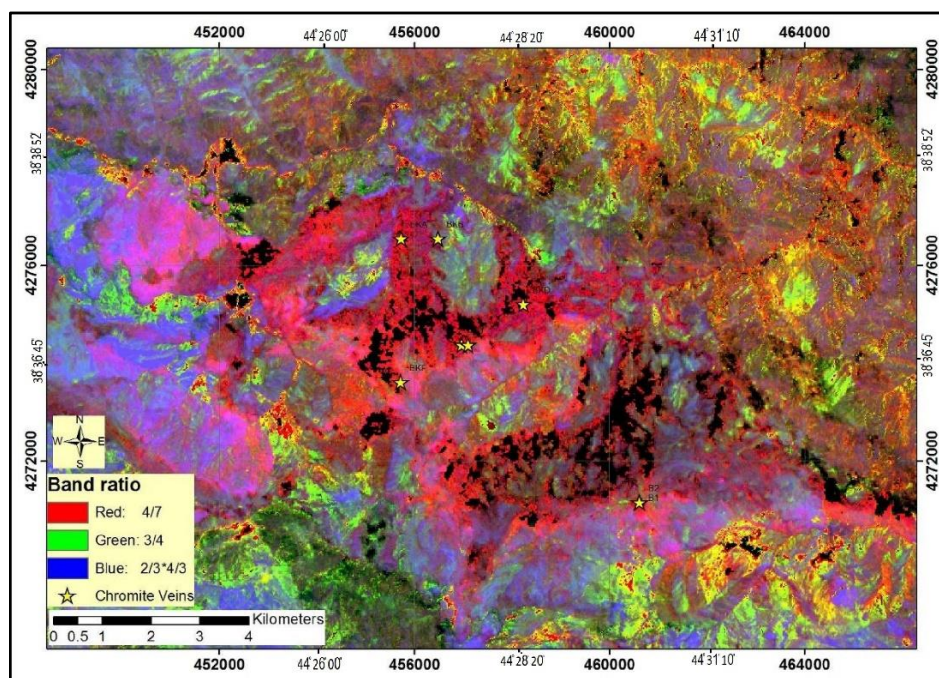
Figure 13. The RGB image of band ratios (4/7), (3/4), (2/3× 4/3) in the study area. Chromite outcrops and veins are shown on the map.
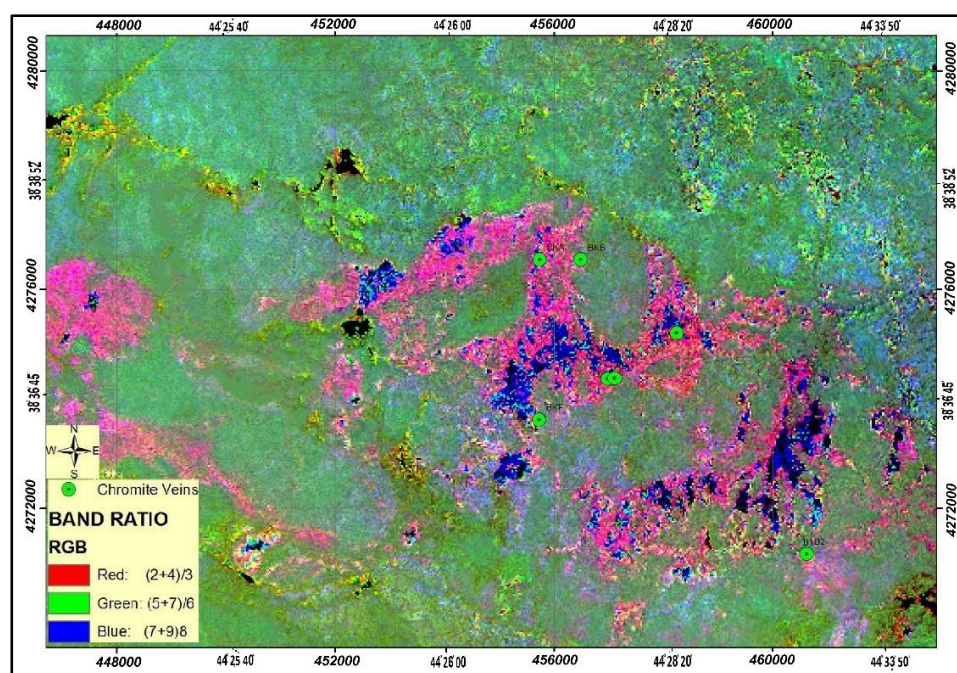

Figure 14. The RGB image of band ratios (2 + 4)/3, (5 + 7)/6, (7 + 9)/8 in the study area. Chromite outcrops and veins are shown on the map.
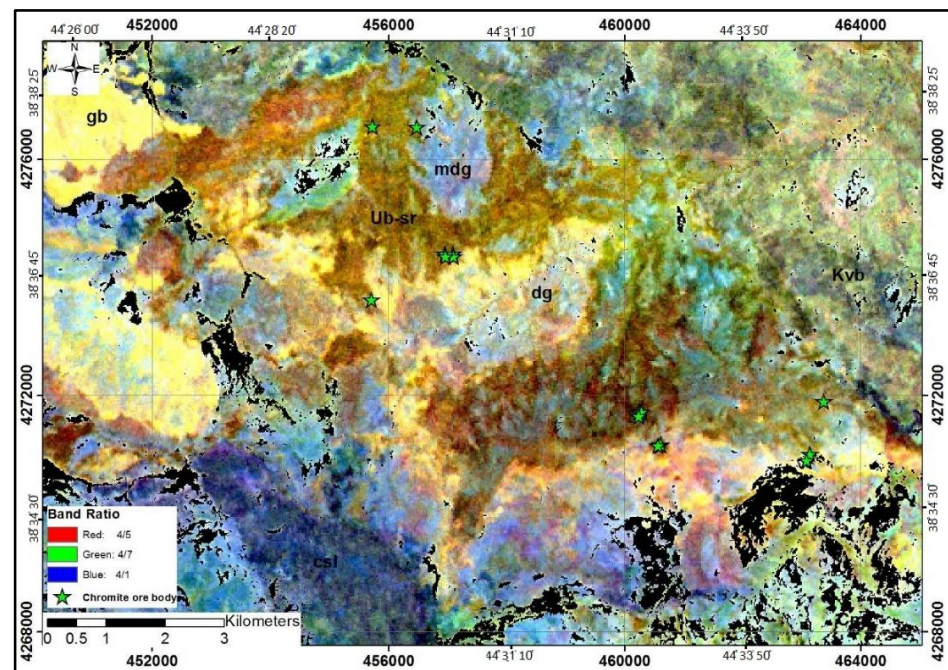
Figure 15. SATER RGB image of band ratios (4/1), (4/5), (4/7) in the study area: Ub-sr—serpentinized ultrabasic; mdg—microdiorite gabbro; dg—diorite gabbro; Cm—conglomerate; Kvb—basalt pillow lava; csl—shale and conglomerate.

6.3. Spectral Angle Mapper

The spectral angle mapper was one of the most useful tools used in this research study. The spectral library, or the spectrum of one of the sufficiently widespread outcrops in the region, was used for prospecting similar spectral pixels. In this method, all pixels were processed and the spectrum of pixels similar to chromite spectra or any other mineral in the region was considered as the objective function.

In the remote sensing studies of Khoy ophiolites there are two major problems that may affect the conclusions of these studies. All the outcrops in this region are very limited, and the chromite masses are in the halo of the dunite, which themselves are enclosed within the harzburgite. Due to the tectonic conditions of this region and the great fractures within it, the dunites and harzburgite are both serpentinized and their separation is practically impossible. In further remote sensing studies, pure spectral pixels were obtained first, and then from five existing anomalies, which were already being mined, the chromite spectra was selected. The result of these procedures is presented in Figures 16–19.
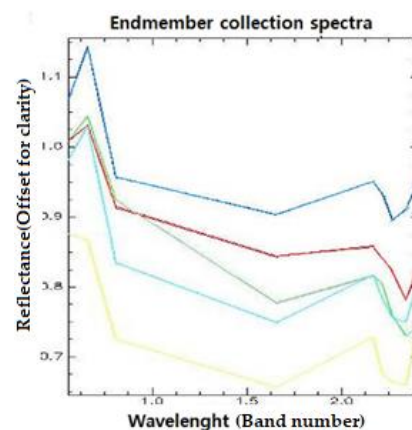

Figure 16. Reflectance spectra of harzburgite exposed at the Khoy ophiolite zone: spectra resampled to ASTER VNIR–SWIR band passes.
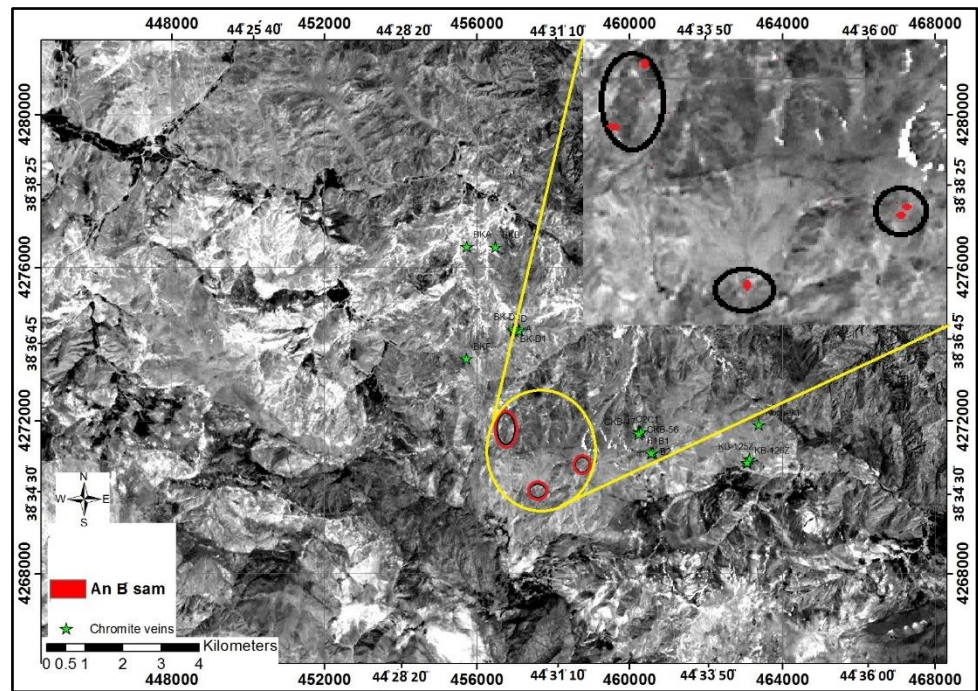
Figure 17. Chromitite-bearing pixels obtained from Anomaly B spectra and SAM in ASTER data.
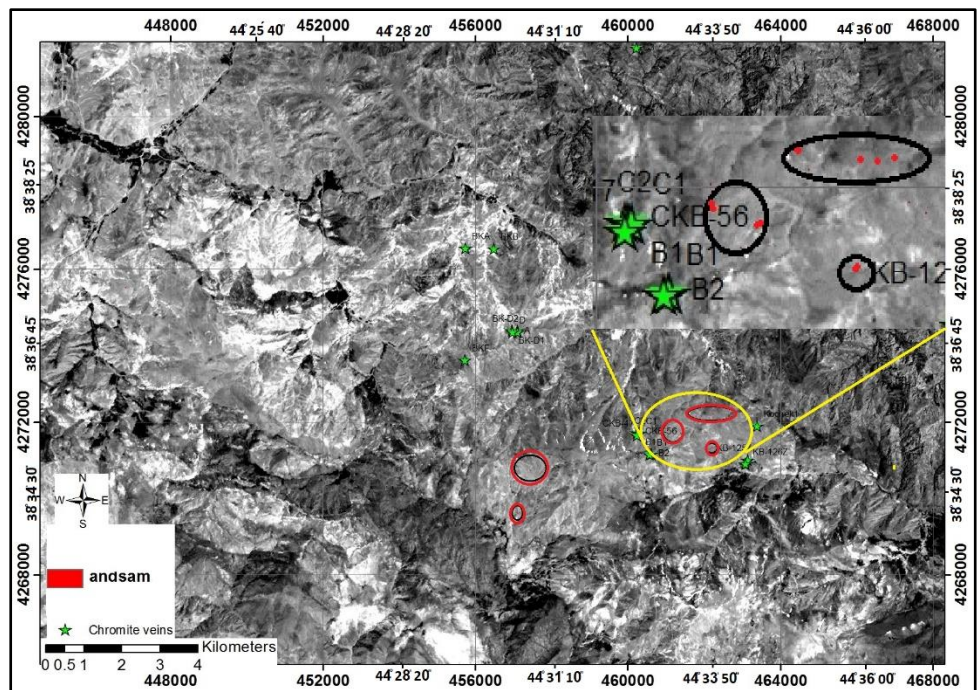

Figure 18. Chromitite-bearing pixels obtained from Anomaly D spectra and SAM in ASTER data.
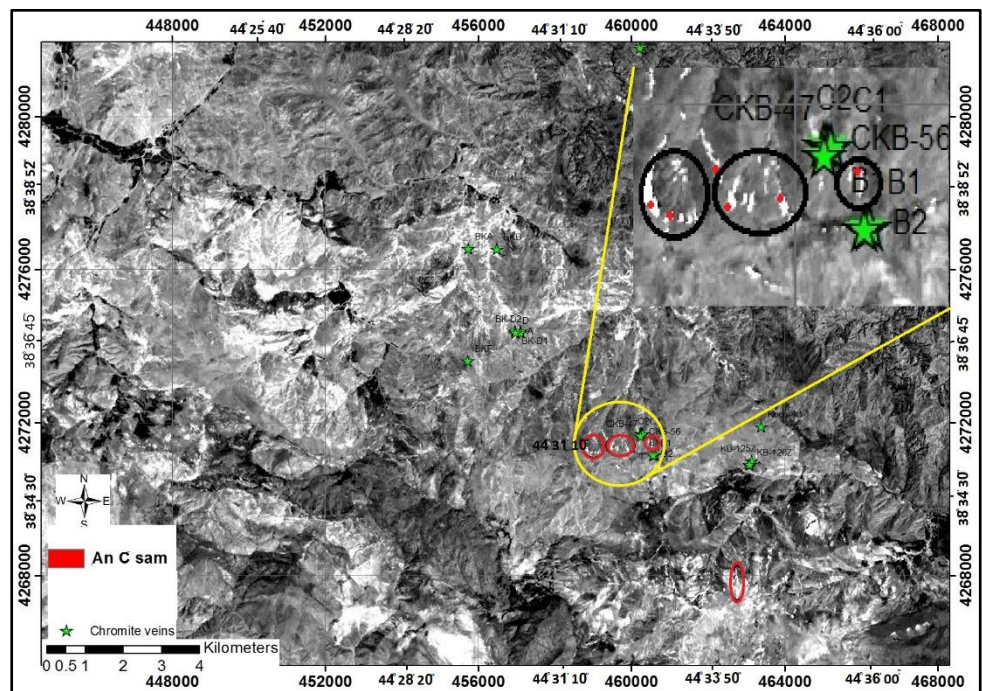
Figure 19. Chromitite-bearing pixels obtained from Anomaly C spectra and SAM in ASTER data.

Finally, with the integration of the obtained data such as the fault map, the separated lithologies, and suitable points from the remote sensing studies and chromite outcrop maps, the most suitable geological traverse lines to continue prospecting in the Khoy ophiolite complex were obtained (Figure 20).
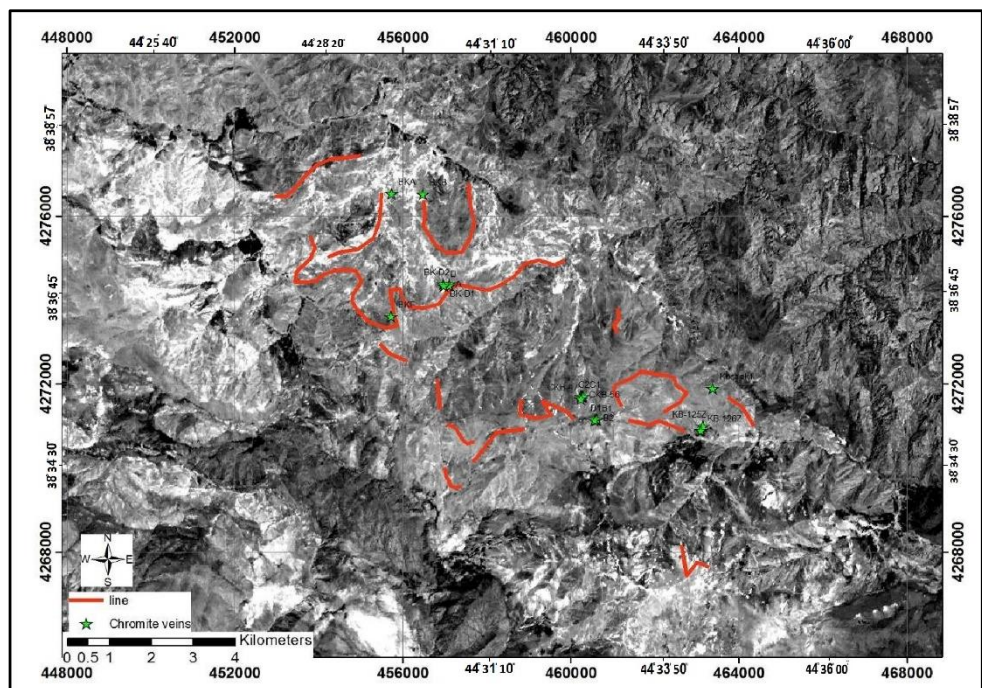

Figure 20. The most suitable geological traverse lines to continue prospecting in the Khoy ophiolite complex.

This leads to the suggestion that geophysical and geochemical studies be conducted in these paths, which pass through some outcrops, for exploration of the greatest number of chromite bodies. As a result, by using remote sensing studies, chromite exploration in ophiolites can be done economically. The prospecting paths, due to the topography of the Khoy ophiolite, are also designed to explore the greatest possible number of chromite lenses. In this way, with the integration of geophysical methods such as gravity and magnetic measurements in the designed paths, desired results can be economically achieved.

7. Conclusions

In this research, VNIR and SWIR bands of ASTER data were used to distinguish lithological units and delineate high-potential chromite mineralized zones in the Khoy ophiolites complex. Harzburgite and dunite are the main units of chromite lens hosts. During this study, using image processing techniques such as the band ratio method, principal component analysis, and the spectral angle mapper algorithm, a large area of these ophiolites was investigated. Consequently, integration of the results derived from the image processing algorithms and other data sets, such as geological maps, can produce accurate information for the reconnaissance stages of chromite exploration at both regional and district scales. This research demonstrates the remote sensing capabilities for the identification of dunite/serpentine or peridotite as host rocks for chromite mineralization in the transition zone of Iranian ophiolitic sequences and lithological mapping in mountainous and inaccessible regions.

References

1. Khan, S.D.; Mahmood, K.; Casey, J.F. Mapping of Muslim Bagh ophiolite complex (Pakistan) using new remote sensing, and field data. *J. Asian Earth Sci.* **2006**, *30*, 333–343. [CrossRef]
2. El-Desoky, H.M.; Soliman, N.; Heikal, M.A.; Abdel-Rahman, A.M. Mapping hydrothermal alteration zones using ASTER images in the Arabian–Nubian Shield: A case study of the northwestern Allaqi District, South Eastern Desert, Egypt. *J. Asian Earth Sci. X* **2021**, *5*, 100060.
3. Hewson, R.D.; Cudahy, T.J.; Mizuhiko, S.; Ueda, K.; Mauger, A.J. Seamless geological map generation using ASTER in the Broken Hill-Curnamona province of Australia. *Remote Sens. Environ.* **2005**, *99*, 159–172. [CrossRef]
4. Mosier, D.L.; Singer, D.A.; Moring, B.C.; Galloway, J.P. Podiform chromite deposits—Database and grade and tonnage models. *US Geol. Surv. Sci. Investig. Rep.* **2012**, *5157*, 45.
5. Imamalipour, A. Geochemistry and geological setting of chromitites of Aland area from the Khoy ophiolite complex, NW Iran. *J. Geosci.* **2011**, *20*, 47–56.
6. Zaeimnia, F.; Kananian, A.; Arai, S.; Mirmohammadi, M.; Imamalipour, A.; Khedr, M.Z.; Miura, M.; Abbou-Kebir, K. Mineral chemistry and petrogenesis of chromitites from the K hoy ophiolite complex, Northwestern Iran: Implications for aggregation of two ophiolites. *Isl. Arc* **2017**, *26*, e12211. [CrossRef]
7. Amer, R.; Kusky, T.; Ghulam, A. Lithological mapping in the Central Eastern Desert of Egypt using ASTER data. *J. Afr. Earth Sci.* **2010**, *56*, 75–82. [CrossRef]
8. Rajendran, S.; Al-Khirbash, S.; Pracejus, B.; Nasir, S.; Al-Abri, A.H.; Kusky, T.M.; Ghulam, A. ASTER detection of chromite bearing mineralized zones in Semail Ophiolite Massifs of the northern Oman Mountains: Exploration strategy. *Ore Geol. Rev.* **2012**, *44*, 121–135. [CrossRef]

9. Rowan, L.C.; Hook, S.J.; Abrams, M.J.; Mars, J.C. Mapping hydrothermally altered rocks at Cuprite, Nevada, using the Advanced Spaceborne Thermal Emission and Reflection Radiometer (ASTER), a new satellite-imaging system. *Econ. Geol.* **2003**, *98*, 1019–1027. [CrossRef]
10. Sabins, F.F. Remote sensing for mineral exploration. *Ore Geol. Rev.* **1999**, *14*, 157–183. [CrossRef]
11. Pournamdari, M.; Hashim, M.; Pour, A.B. Spectral transformation of ASTER and Landsat TM bands for lithological mapping of Soghan ophiolite complex, south Iran. *Adv. Space Res.* **2014**, *54*, 694–709. [CrossRef]
12. Pournamdari, M.; Hashim, M. Detection of chromite bearing mineralized zones in Abdasht ophiolite complex using ASTER and ETM+ remote sensing data. *Arab. J. Geosci.* **2014**, *7*, 1973–1983. [CrossRef]
13. Crosta, A.P.; De Souza Filho, C.R.; Azevedo, F.; Brodie, C. Targeting key alteration minerals in epithermal deposits in Patagonia, Argentina, using ASTER imagery and principal component analysis. *Int. J. Remote Sens.* **2003**, *24*, 4233–4240. [CrossRef]
14. Massironi, M.; Bertoldi, L.; Calafa, P.; Visonà, D.; Bistacchi, A.; Giardino, C.; Schiavo, A. Interpretation and processing of ASTER data for geological mapping and granitoids detection in the Saghro massif (eastern Anti-Atlas, Morocco). *Geosphere* **2008**, *4*, 736–759. [CrossRef]
15. Abdeen, M.M.; Allison, T.K.; Abdelsalam, M.G.; Stern, R.J. Application of ASTER band-ratio images for geological mapping in arid regions; the Neoproterozoic Allaqi Suture, Egypt. *Abstr. Program Geol. Soc. Am.* **2001**, *3*, 289.
16. Yamaguchi, Y.; Naito, C. Spectral indices for lithologic discrimination and mapping by using the ASTER SWIR bands. *Int. J. Remote Sens.* **2003**, *24*, 4311–4323. [CrossRef]
17. Crawford, A.R. Possible impact structure in India. *Nature* **1972**, *237*, 96. [CrossRef]
18. Khalatbari-Jafari, M.; Juteau, T.; Bellon, H.; Emami, H. Discovery of two ophiolite complexes of different ages in the Khoy area (NW Iran). *Comptes Rendus Geosci.* **2003**, *335*, 917–929. [CrossRef]
19. Pessagno, E.A.; Ghazi, A.M.; Kariminia, M.; Duncan, R.A.; Hassanipak, A.A. Tectonostratigraphy of the Khoy complex, northwestern Iran. *Stratigraphy* **2005**, *2*, 49–63.
20. Hunt, G.R.; Ashley, R.P. Spectra of altered rocks in the visible and near-infrared. *Econ. Geol.* **1979**, *74*, 1613–1629. [CrossRef]
21. Abrams, M.; Hook, S.J. Simulated ASTER data for geologic studies. *IEEE Trans. Geosci. Remote Sens.* **1995**, *33*, 692–699. [CrossRef]
22. Gad, S.; Kusky, T. ASTER spectral for lithological mapping in the Arabian–Nubian Shield, the Neoproterozoic Wadi Kid area, Sinai, Egypt. *Gondwana Res.* **2007**, *11*, 326–335. [CrossRef]
23. Gabr, S.; Ghulam, A.; Kusky, T. Detecting areas of high-potential gold mineralization using ASTER data. *Ore Geol. Rev.* **2010**, *38*, 59–69. [CrossRef]
24. Moore, F.; Rastmanesh, F.; Asadi, H.; Modabberi, S. Mapping mineralogical alteration using principal-component analysis and matched filter processing in the Takab area, north-west Iran, from ASTER data. *Int. J. Remote Sens.* **2008**, *29*, 2851–2867. [CrossRef]
25. Rajendran, S.; Nasir, S. Mapping of Moho and Moho Transition Zone (MTZ) in Samail ophiolites of Sultanate of Oman using remote sensing technique. *Tectonophysics* **2015**, *657*, 63–80. [CrossRef]
26. Goetz, A.F.; Rock, B.N.; Rowan, L.C. Remote sensing for exploration; an overview. *Econ. Geol.* **1983**, *78*, 573–590. [CrossRef]
27. Sultan, M.; Arvidson, R.E.; Sturchio, N.C. Mapping of serpentinites in the Eastern Desert of Egypt by using Landsat thematic mapper data. *Geology* **1986**, *14*, 995–999. [CrossRef]
28. Nidamanuri, R.R.; Ramiya, A.M. Spectral identification of materials by reflectance spectral library search. *Geocarto Int.* **2014**, *29*, 609–624. [CrossRef]
29. Galvao, L.S.; Formaggio, A.R.; Tisot, D.A. Discrimination of sugarcane varieties in Southeastern Brazil with EO-1 Hyperion data. *Remote Sens. Environ.* **2005**, *94*, 523–534. [CrossRef]
30. Ninomiya, Y.; Fu, B.; Cudahy, T.J. Detecting lithology with Advanced Spaceborne Thermal Emission and Reflection Radiometer (ASTER) multispectral thermal infrared "radiance-at-sensor" data. *Remote Sens. Environ.* **2005**, *99*, 127–139. [CrossRef]
31. Pour, A.B.; Hashim, M. ASTER, ALI, and Hyperion sensors data for lithological mapping and ore minerals exploration. *SpringerPlus* **2014**, *3*, 1–9.
32. Rashmi, S.; Addamani, S.; Ravikiran, A. Spectral Angle Mapper Algorithm for Remote Sensing Image Classification. *Ijiset Int. J. Innov. Sci. Eng. Technol.* **2014**, *1*, 5481.
33. Kamal, M.; Phinn, S. Hyperspectral data for mangrove species mapping: A Comparison of pixel-based object-based approach. *Remote Sens.* **2011**, *3*, 2222–2242.
34. Benomar, T.B.; Fuling, B. Improved geological mapping using Landsat-5 TM data in Weixi area, Yunnan province China. *GeoSpat. Inf. Sci.* **2005**, *8*, 110–114. [CrossRef]
35. Harrison, S. Standardized principal component analysis. *Int. J. Remote Sens.* **1985**, *6*, 883–890.
36. Kruse, F.A.; Lefkoff, A.B.; Boardman, J.W.; Heidebrecht, K.B.; Shapiro, A.T.; Barloon, P.J.; Goetz, A.F. The spectral image processing system (SIPS)—interactive visualization and analysis of imaging spectrometer data. *Remote Sens. Environ.* **1993**, *44*, 145–163. [CrossRef]